HHS Public Access

Author manuscript

Nat Neurosci. Author manuscript; available in PMC 2010 November 01.

Published in final edited form as:

Nat Neurosci. 2010 May ; 13(5): 592–600. doi:10.1038/nn.2517.

Reduction in endocannabinoid tone is a homeostatic mechanism for specific inhibitory synapses

Jimok Kim[1] and **Bradley E. Alger**[1,2,3]

[1] Department of Physiology, University of Maryland School of Medicine, 655 W. Baltimore St., Baltimore, MD 21201, USA

[2] Department of Psychiatry, University of Maryland School of Medicine, 655 W. Baltimore St., Baltimore, MD 21201, USA

[3] Program in Neuroscience, University of Maryland School of Medicine, 655 W. Baltimore St., Baltimore, MD 21201, USA

Abstract

When chronic alterations in neuronal activity occur, network gain is maintained by global homeostatic scaling of synaptic strength, but the stability of microcircuits can be controlled by unique adaptations that differ from the global changes. It is not understood how specificity of synaptic tuning is achieved. Here we report that, while a large population of inhibitory synapses is homeostatically scaled down after chronic inactivity, decreased endocannabinoid tone specifically strengthens a subset of GABAergic synapses that express cannabinoid receptors. In hippocampal slice cultures of rats, a 3–5 day blockade of neuronal firing facilitates uptake and degradation of anandamide. The consequent reduction in basal stimulation of cannabinoid receptors augments GABA release probability, thus fostering rapid depression of synaptic inhibition and on-demand disinhibition. This novel regulatory mechanism, mediated by activity-dependent changes in tonic endocannabinoid level, permits selective local tuning of inhibitory synapses in hippocampal networks.

Signaling gain within a neuronal network can be maintained during long-lasting activity alterations by homeostatic compensation of synaptic strengths[1]. However, unchecked, global homeostatic scaling of synapses may destabilize a network, because of complexities in realistic circuits[2]–[4]. As a compromise between gain and stability, subsets of circuits are often maintained by adaptations opposite to simple homeostatic scaling[4]–[7]. A complete understanding of adaptive plasticity requires knowing how subsets of synapses can diverge from “conventional” homeostatic adaptations.

In a conventional homeostatic paradigm, days-long inactivity strengthens excitatory synapses and weakens inhibitory synapses for compensatory boosting of net excitability[1], [8].

Correspondence should be addressed to B.E.A. (balgerlab@gmail.com) (Phone 410-706-3350; Fax 410-706-8341).

AUTHOR CONTRIBUTIONS

J.K. and B.E.A. designed the research and wrote the manuscript. J.K. conducted the experiments.

Therefore, changes in synaptic strengths opposite to the conventional ones could be classified as “inverse-homeostatic” scaling: e.g., inactivity-induced decreases in glutamatergic transmission or increases in γ-aminobutyric acid (GABA) transmission. For example, a CA3 microcircuit can be stabilized by inverse-homeostatic down-regulation of recurrent glutamatergic synapses[4]. Optimal efficiency of hippocampal circuits after inactivity can also be achieved by balanced strengthening of both excitatory and inhibitory synapses, with the latter effect representing an inverse homeostatic change[5–7]. The accumulating evidence for critical roles of inverse-homeostatic changes in local network adaptations necessitates a better understanding of the mechanisms involved.

Given the functional diversity of hippocampal interneurons, a global and uniform synaptic scaling might not suffice for homeostatic maintenance of the inhibitory circuits. This led us to examine specificity of homeostatic plasticity at inhibitory synapses, focusing on the role of endocannabinoids, which directly regulate only GABAergic terminals that contain cannabinoid receptor type 1 (CB1Rs). We hypothesized that an inactivity-induced change in endocannabinoid function mediates homeostasis of CB1R-positive inhibitory synapses, perhaps in parallel with global and conventional synaptic scaling. Endocannabinoids, anandamide and 2-arachidonoyl glycerol (2-AG), are produced upon a rise in Ca^{2+} and/or activation of G proteins, and suppress synaptic transmission by binding to presynaptic CB1Rs[9, 10]. Several properties of the endocannabinoids and CB1R led us to postulate their involvement in adaptation of inhibitory circuits. First, most CB1Rs in the hippocampus are expressed on GABAergic terminals that contain cholecystokinin, but not parvalbumin[11, 12]. Second, CB1Rs undergo long-lasting changes when neuronal activity is altered by epilepsy[13, 14] or by chronic application of CB1R agonists[15, 16]. Third, the action of endocannabinoids is very local and specific because of temporal and spatial limitations on their production and extracellular spread. Fourth, endocannabinoids are produced in proportion to the degree of neuronal activity, hence the endocannabinoid system is ideally suited to serve the demands of homeostasis, an activity-dependent process. We studied adaptive plasticity of inhibitory transmission in hippocampal slice cultures, which preserve realistic circuits, and yet are amenable to long-term manipulations.

Here we show that the release probability (P_r) of GABA at CB1R-positive inhibitory synapses is augmented after chronic activity deprivation induced by tetrodotoxin (TTX). The inactivity-induced strengthening of GABAergic synapses is mediated by reduced tonic action of anandamide, rather than 2-AG. Anandamide tone is decreased by upregulation of transport and degradation.

RESULTS

Homeostatic plasticity of GABAergic synapses

We first examined the ability of rat hippocampal organotypic slice cultures to express homeostatic plasticity of inhibitory synapses when neuronal firing was blocked with 1 μM TTX for 3–5 days. The mean amplitude of miniature inhibitory postsynaptic currents (mIPSCs) recorded from CA1 pyramidal neurons was significantly smaller in TTX-treated cells (−58 ± 6 pA, n = 7) than in control cells (−91 ± 9 pA, n = 7) ($P < 0.01$, t-test; Fig. 1a), as found with cultured neurons[17, 18]. The mean mIPSC frequency was unaffected: 3.9 ± 0.9

Hz for control and 3.4 ± 0.5 Hz for TTX-treated cells ($P > 0.5$, t-test; Fig. 1a). The decrease in mIPSC amplitude is consistent with inactivity-induced homeostasis. If the scaling of mIPSCs applied to all inhibitory synapses, the distributions of mIPSC amplitudes of control and TTX-treated cells would be identical after the control population was adjusted by a scaling factor[18, 19]. Indeed, when each control mIPSC was scaled down (see Methods), the adjusted control and TTX-treated mIPSC distributions overlapped almost perfectly ($P > 0.9$, Kolmogorov-Smirnov test; Fig. 1b). Hence, chronic TTX scaled down the whole population of mIPSCs, and not just a subset.

We next examined whether the amplitudes of evoked IPSCs (eIPSCs), which are action potential- and Ca^{2+}-dependent, were also reduced by chronic TTX. TTX was removed from the cultures before testing in eIPSC experiments. Using "minimal stimulation"[20], we recorded unitary IPSCs (uIPSCs) as a measure of release from putative single axons (Fig. 1c–e). Since synaptic homeostasis is synapse-specific[4, 21, 22], we segregated different types of inhibitory synapses according to the Ca^{2+} channels utilized for transmission: most inhibitory neurons in hippocampal slices use N-type or P/Q-type Ca^{2+} channels but not both[23]. Synapses using P/Q-type Ca^{2+} channels were isolated by preincubating slice cultures with 500 nM ω-conotoxin GVIA, an irreversible N-type Ca^{2+} channel blocker. The control mean amplitude of conotoxin-resistant uIPSCs (excluding failures) was −582 ± 123 pA (n = 6) and was significantly reduced by chronic TTX to −183 ± 17 pA (n = 5) ($P < 0.02$, t-test; Fig. 1c,**e**). Similarly, in slices preincubated with 300 nM ω-agatoxin IVA (irreversible P/Q type Ca^{2+} channel blocker), the mean amplitude of uIPSCs (excluding failures) was decreased by chronic inactivity: from −442 ± 48 pA (n = 5, control) to −196 ± 46 pA (n = 6, TTX-treated, $P < 0.01$, t-test; Fig. 1d,e). The decreases in amplitudes of mIPSCs and uIPSCs both conform to conventional homeostatic scaling induced by inactivity.

Network excitability, a target for homeostatic control, is determined in part by on-going GABA release: mIPSCs and spike-driven spontaneous IPSCs (sIPSCs). We therefore measured sIPSC frequency, again separating conotoxin- and agatoxin-resistant synapses. After recording a mixture of mIPSCs and sIPSCs, only mIPSCs were recorded from the same cell in 0.5 μM TTX. The mIPSC frequency was subtracted from the total of mIPSC plus sIPSC to obtain the frequency of sIPSC only (Fig. 2a–c). For conotoxin-resistant synapses, the sIPSC frequency of TTX-treated neurons (0.07 ± 0.03 Hz; n = 5) was lower than that of controls (0.26 ± 0.05 Hz; n = 6) ($P < 0.02$, t-test; Fig. 2a,**c**), as expected for conventional homeostatic downregulation of inhibitory synapses. For agatoxin-resistant synapses, however, activity deprivation increased the sIPSC frequency from 0.10 ± 0.04 Hz (five control cells) to 0.74 ± 0.11 Hz (five TTX-treated cells) ($P < 0.0005$, t-test; Fig. 2b,**c**).

Because the increased frequency of agatoxin-resistant sIPSCs was unexpected, we asked if other properties of Ca^{2+}-dependent GABA release are also at variance with conventional synaptic homeostasis. Ca^{2+}-dependent transmission is governed by P_r, which can be assessed with short-term plasticity, or paired-pulse ratio (PPR): generally, P_r is inversely related to PPR. To measure P_r, we evoked IPSCs by delivering three stimuli at 20 Hz to CA1 stratum pyramidale. At conotoxin-resistant synapses, eIPSC depression in control cells (n = 6) was similar to that in TTX-treated cells (n = 6) ($P > 0.2$, two-way ANOVA; Fig. 2d), suggesting P_r is unaltered by chronic inactivity. In contrast, agatoxin-resistant eIPSCs

showed greater depression in TTX-treated neurons (n = 24) than in control cells (n = 30) (Fig. 2e; $P < 0.001$ at each eIPSC number, Bonferroni t-test after two-way ANOVA). The amplitude of the third eIPSC, normalized to the first, was 53 ± 2% in control and 38 ± 1% in TTX-treated cells. This indicates that P_r was actually increased at the agatoxin-resistant synapses. To crosscheck this conclusion, we estimated changes in P_r with an independent method by analyzing the coefficient of variation (CV) of uIPSCs and got the same result (Supplementary Fig. 1).

In hippocampus, one of the major differences between agatoxin-resistant and conotoxin-resistant GABAergic synapses is that only the former possess CB1Rs[24]. We confirmed that the conotoxin-resistant synapses were insensitive to depolarization-induced suppression of IPSC (DSI), a short-term synaptic plasticity mediated by endocannabinoid (Supplementary Fig. 2). To account for the increase in basal P_r found specifically at agatoxin-resistant, CB1R-positive synapses, we hypothesized that the chronic inactivity might reduce a persistent, "tonic," endocannabinoid action and diminish basal CB1R activation.

Activity deprivation reduces basal activation of CB1R

To test the above hypothesis, we first determined whether tonic activation of CB1R is affected by TTX treatment. If the basal CB1R activation, hence a tonic brake on GABA release, is lowered by inactivity, a CB1R antagonist would increase eIPSC amplitude to a lesser extent in TTX-treated cells than in control cells. In this and subsequent eIPSC recordings, slices were preincubated with 300 nM ω-agatoxin IVA for 15–30 min to isolate CB1R-positive terminals. In control cells, CB1R antagonist (either 2 μM SR141716 or 2 μM AM251) enhanced eIPSC amplitudes by 66 ± 10% (n = 13), but in TTX-treated cells (n = 12) only by 19 ± 2% (Fig. 3a). The effects of SR141716 (n = 7 for both control and TTX-treated groups) were not significantly different from those of AM251 (n = 6 for control and 5 for TTX) ($P > 0.5$, t-tests; Fig. 3a inset), thus the data obtained with the two antagonists were pooled. The similarity of effects of the two CB1R antagonists indicates that they were specifically mediated by CB1Rs (see also Supplementary Fig. 3). The significantly smaller effect of CB1R antagonists in TTX-treated cells ($P < 0.01$, t-test) suggests that the tonic activation of CB1R was diminished by chronic inactivity.

To distinguish between the CB1R-antagonist and inverse-agonist effects of SR141716 and AM251, we removed Ca^{2+} from the pipette solution while keeping the concentration of free EGTA at 1.7 mM (same free EGTA as in Fig. 3a) to prevent tonic release of endocannabinoids[25], without interfering with CB1Rs. With this "zero-Ca^{2+}" pipette solution, SR141716 (2 μM) failed to increase the eIPSC amplitude (107 ± 5% of baseline; n = 7; $P > 0.4$, paired t-test) (Fig. 3b), yet if SR141716 had increased eIPSCs by an inverse-agonist action, the effect would have persisted. We conclude that SR141716 increases eIPSCs by antagonizing CB1Rs that are persistently activated by endocannabinoid binding. This result also demonstrates that the tonic CB1R activation occurs via endocannabinoids released only from the recorded postsynaptic pyramidal cell, and not those from other cells.

Because CV of eIPSC amplitudes is a presynaptic property, the CV^{-2} would increase if a presynaptic mechanism increased the eIPSC amplitude[26]. Analysis of the changes in CV^{-2} and eIPSC amplitudes caused by CB1R antagonists implies the drugs act presynaptically

(Fig. 3c). We also probed this issue with PPR. If an increase in eIPSC amplitudes is caused by presynaptic enhancement of P_r, increases in eIPSCs should be proportional to increases in PPR^{-1}, because P_r is inversely related to PPR. We evoked three IPSCs at 20 Hz and used the third eIPSC amplitude, normalized to the first eIPSC, to calculate PPR3 (= IPSC3/IPSC1). The larger increase in eIPSC was accompanied by a larger increase in $PPR3^{-1}$ (representing P_r) in control cells than in TTX-treated cells (Fig. 3d). This result also argues that the increase in eIPSC amplitudes caused by CB1R antagonists was mediated by a presynaptic mechanism, probably an increase in P_r. Finally, if tonic activation of CB1R determines the basal P_r of GABAergic synapses, the effect of CB1R antagonists will be larger at synapses with lower P_r (because these synapses will be more depressed by endocannabinoid tone). Indeed, the degree of eIPSC enhancement induced by CB1R antagonists was proportional to PPR3, where a low value of PPR3 implies a high basal P_r (Fig. 3e), indicating that the basal P_r is largely influenced by tonic activation of CB1R. Additional evidence presented below argues that the difference in the ability of CB1R antagonists to increase eIPSCs is attributable to alterations in the endocannabinoid system, rather than other potential effects of chronic inactivity (see Discussion).

One possibility for the reduced tonic CB1R activation is that the receptors could have become less responsive to endocannabinoids because of changes in receptor density or sensitivity. To assess CB1R responsiveness, we measured eIPSC suppression by WIN55212-2, a synthetic agonist resistant to cellular uptake. In controls, WIN55212-2 reduced the eIPSC amplitude to 46 ± 5% of baseline at 5 nM (n = 7), 28 ± 5% at 20 nM (n = 7), and 9 ± 2% at 200 nM (n = 7) (Fig. 4a,**b**). The effect of WIN55212-2 in TTX-treated cells was not significantly different at any concentration from that in control cells ($P > 0.4$ at each concentration, t-tests). WIN55212-2 suppressed the TTX-treated eIPSCs to 50 ± 9% (5 nM; n = 7), 23 ± 5% (20 nM; n = 6), and 10 ± 3% (200 nM; n = 7) of the baseline. Therefore, CB1R responsiveness is not altered by activity deprivation.

Basal $[Ca^{2+}]$ and Ca^{2+}-dependent 2-AG release are unaltered

Because postsynaptic basal Ca^{2+} is a crucial factor for tonic release of endocannabinoid (Fig. 3b)[25], we hypothesized that chronic TTX might reduce the postsynaptic basal $[Ca^{2+}]_{in}$. When measured with Fura-2 (200 μM), the mean basal $[Ca^{2+}]_{in}$ in somata of control pyramidal neurons was 40 ± 7 nM (n = 9), similar to 31 ± 4 nM in TTX-treated cells (n = 8) ($P > 0.2$, t-test; Fig. 5a,**b**). This implies that one factor in tonic endocannabinoid production – basal $[Ca^{2+}]_{in}$ – is not affected by chronic TTX, but does not rule out other changes, e.g., Ca^{2+} sensitivity of synthetic enzyme(s).

To assay the Ca^{2+} sensitivity of endocannabinoid production, we elevated $[Ca^{2+}]_{in}$ by depolarizing pyramidal cells to 0 mV for 500 ms, while monitoring endocannabinoid action. There was no difference in the peak $[Ca^{2+}]_{in}$ (5-s time window) following the depolarization in control (116 ± 20 nM) and TTX-treated cells (111 ± 12 nM) ($P > 0.8$, t-test; Fig. 5a,**b**). However, our 1 Hz sampling rate might have missed a difference in $[Ca^{2+}]_{in}$ within the first 1-s bin. The effect of endocannabinoid after the depolarization was assayed as DSI, simultaneously with Ca^{2+} imaging (Fig. 5c). DSI was quantified by integrating the suppression of eIPSC amplitudes from 6 to 144 s after the depolarization. The DSI induced

by 500 ms depolarization was not significantly different between control (890 ± 220 %·s; n = 9) and TTX-treated cells (1,270 ± 320 %·s; n = 8) ($P > 0.3$, t-test). Peak suppression of the eIPSC, taken as the average of the second and third eIPSCs after depolarization, was also similar: 25 ± 6% reduction in control and 34 ± 5% in TTX-treated cells ($P > 0.2$, t-test). When greater Ca^{2+} influx was induced in the postsynaptic cells with longer (5 s) depolarizations, DSI integrated over 4 min still did not show any difference (Fig. 5d,**e**): 5,150 ± 400 %·s in 14 control cells and 4,250 ± 620 %·s in 11 TTX-treated cells ($P > 0.2$, t-test). Because DSI is mediated by 2-AG[10], this result indicates that the Ca^{2+} sensitivity of 2-AG production was not affected by chronic inactivity. In conclusion, the activity deprivation affects neither basal $[Ca^{2+}]_{in}$, depolarization-induced $[Ca^{2+}]_{in}$ elevation, nor Ca^{2+}-dependence of 2-AG mobilization.

Tonic uptake and degradation of anandamide are enhanced

Lack of changes in CB1R, or endocannabinoid production and release, prompted us to examine whether tonic uptake and degradation of endocannabinoid were altered by chronic TTX. Chronic inactivity might enhance uptake of basal endocannabinoid and thereby reduce endocannabinoid tone. This predicts that inhibition of transport by AM404 would cause a greater increase in endocannabinoid tone in TTX-treated slices than in control slices. As predicted, the eIPSC suppression induced by 20 μM AM404 was significantly larger in TTX-treated neurons (27 ± 7%; n = 7) than in control cells (2 ± 2% increase; n = 6) ($P < 0.005$, t-test; Fig. 6a). This result suggests that the chronic inactivity facilitates tonic endocannabinoid uptake.

If 2-AG is tonically released and chronic inactivity increases the rate of 2-AG uptake, then DSI decay would be accelerated because the 2-AG released during DSI would be inactivated more rapidly[27–29]. In contrast to this prediction, the DSI time courses were not different between the two groups (Fig. 5c–**e**), and the similarity persisted when 2-AG uptake was blocked by AM404 (Fig. 6b). We confirmed that AM404 effectively blocked 2-AG uptake because AM404 prolonged DSI decay rate ($P < 0.002$, t-tests between AM404 and no-AM404; Fig. 6c). Nevertheless, DSI integrals after 5-s depolarizations were indistinguishable between control (8,990 ± 670 %·s; n = 5) and TTX-treated (9,120 ± 110 %·s; n = 5) groups in the presence of 20 μM AM404 ($P > 0.9$, t-test; Fig. 6b,**c**). Thus, neither production nor uptake of 2-AG during DSI is altered by chronic inactivity.

Since activity deprivation affected tonic endocannabinoid actions, but not 2-AG signaling, we postulated that anandamide, rather than 2-AG, is tonically released. Although the endocannabinoid transporter has the same binding affinity for 2-AG and anandamide, the driving force for uptake of a given endocannabinoid can be selectively increased if intracellular degradation of that endocannabinoid is enhanced[30]. If anandamide accounts for the tonic endocannabinoid effects, the activity of its degradative enzyme (fatty acid amide hydrolase; FAAH), hence the driving force for anandamide uptake, might be higher in TTX-treated cells than in control cells. This hypothesis predicts that blockade of FAAH would cause greater accumulation of extracellular anandamide, and consequently a greater CB1R-dependent eIPSC suppression, in activity-deprived cells than in control cells. To test this, we measured eIPSC reduction caused by 1 μM URB597, a very specific and potent inhibitor of

FAAH[31]. As predicted, the URB597-mediated depression of eIPSC was significantly larger in TTX-treated cells (44 ± 6%; n = 7) than in controls (15 ± 8%; n = 6) ($P < 0.02$, t-test; Fig. 6d). URB597 had no effect on 2-AG signaling, as it did not affect DSI (Supplementary Fig. 4)[27, 28]. These results suggest that chronic inactivity boosts FAAH activity, which in turn causes stronger uptake of tonically released anandamide.

We next tested whether AM404 and URB597 suppressed eIPSCs by a presynaptic mechanism. Because the eIPSC reduction caused by AM404 was not significantly different from that caused by URB597 ($P > 0.05$, t-tests) in either control or TTX-treated cell, the data from AM404 and URB597 experiments were pooled in the following analyses (Fig. 6e,**f**). We first plotted changes in CV^{-2} caused by AM404 or URB597 against changes in eIPSC amplitudes. Indeed, eIPSC amplitudes and CV^{-2} decreased proportionately (Fig. 6e), which is consistent with presynaptic mechanism. Next, we compared $PPR3^{-1}$ changes in control and TTX-treated neurons. In TTX-treated cells, AM404 or URB597 caused larger decreases in both eIPSC amplitude and $PPR3^{-1}$ than they did in control cells (Fig. 6f), suggesting that they acted presynaptically, potentially by decreasing P_r. In the third test, we asked if AM404 and URB597 suppressed eIPSCs via presynaptic CB1Rs. In the presence of SR14176 (2 μM), a cocktail of AM404 (20μM) and URB597 (1 μM) did not reduce eIPSC amplitudes (100 ± 3% of baseline; n = 6; Fig. 6g) ($P > 0.5$, paired t-test), indicating that the effects of these drugs were mediated by CB1Rs.

The effect of URB597 (Fig. 6d) suggests that FAAH activity had been increased. We further assayed FAAH activity by bath-applying anandamide, a substrate for FAAH, at a submaximal concentration (720 nM) while monitoring eIPSC amplitudes. We used the zero-Ca^{2+} pipette solution (as in Fig. 3b) to prevent formation of endogenous anandamide and leave FAAH unoccupied. If FAAH were more active, e.g., in TTX-treated cells, bath-applied anandamide would be less effective in suppressing eIPSCs. The reduction in eIPSC caused by 720 nM anandamide was significantly smaller in TTX-treated cells (22 ± 6%; n = 5) than in controls (46 ± 6%; n = 5) ($P < 0.05$, t-test; Fig. 6h), suggesting that FAAH is more active in TTX-treated cells.

Deafferentation also decreases endocannabinoid tone

To simulate a more realistic model of activity loss than chronic TTX, we imposed neuronal inactivity by deafferentation, which may be more relevant to in vivo pathology. Afferent excitation of the CA1 region was reduced by a surgical removal of the CA3 area, the major source of excitatory inputs to CA1. In control slices, a cut was made between CA1 and subiculum, which is on the efferent side of CA1 (Fig. 7a). Evoked IPSCs were recorded from CA1 pyramidal neurons 5–7 days after the cut. We performed a series of experiments that were similar to those in Figure 3 to examine whether chronic deafferentation induced changes similar to those caused by TTX treatment.

As in TTX-treated slices, eIPSCs in deafferented slices showed more pronounced short-term depression than those in control slices (Fig. 7b). The mean PPR3 was 49 ± 3% (n = 7) in control cells and 39 ± 2% (n = 6) in deafferented cells ($P < 0.01$, Bonferroni t-test after two-way ANOVA). In addition, SR141716 (2 μM) enhanced eIPSCs in deafferented neurons by 13 ± 4% (n = 6), which is significantly smaller than in control cells (49 ± 9%; n = 7) ($P <$

0.005, t-test; Fig. 7c). Finally, we observed that basal P_r, as represented by PPR3, is related to the basal activation of CB1Rs (Fig. 7d). These tests show that the deafferentation, like chronic TTX, reduced endocannabinoid tone. Additional tests, analogous to those carried out earlier for TTX-treated slices, revealed that the effects of SR141716 are mediated presynaptically (Fig. 7e,f; see legend for details). These results therefore demonstrate that the endocannabinoid tone can be regulated by pathologically relevant inactivity such as neurodegeneration, and support the use of chronic TTX treatment as a model for studying the mechanisms involved.

Role of the increased GABAergic P_r in network integration

The roles of the reduced endocannabinoid tone in maintaining network activity should be interpreted in conjunction with its effects on excitatory synapses, because CB1Rs are also expressed on glutamatergic terminals at a low level[12, 32]. We therefore examined the effect of SR141716 on evoked excitatory postsynaptic currents (eEPSCs). Bath-applied 2 μM SR141716 did not change the amplitudes of eEPSCs in either control (6 ± 6% reduction; n = 5) or TTX-treated cells (8 ± 3% reduction; n = 5) ($P > 0.09$, paired t-test each for control or TTX-treated group; Fig. 8a,**b**). This indicates that the basal anandamide does not participate in homeostatic scaling of eEPSCs.

We next examined changes in short-term plasticity of eEPSCs. In control cells (n = 5), EPSCs evoked three times at 20 Hz initially displayed a slight facilitation (109 ± 7% of the first EPSC) and then a mild depression (87 ± 7%) (Fig. 8c). In contrast, eEPSCs in TTX-treated neurons (n = 8) depressed more than control eEPSCs (83 ± 3% and 63 ± 4% for the second and third EPSCs respectively) ($P < 0.005$ at each eEPSC number, Bonferroni t-test after two-way ANOVA). This result indicates that glutamatergic P_r is also increased after chronic inactivity, but independently of the tonic anandamide actions, as it was not altered by SR141716 in either TTX-treated or control groups ($P > 0.8$, paired t-tests; Fig. 8d). Although the increase in P_r of CB1R-positive inhibitory synapses after activity deprivation seems contrary to conventional homeostatic scaling, the consequent enhancement of GABAergic short-term depression (Fig. 2d) will dampen excitatory transmission to a lesser degree at high frequency transmission (20 Hz). Such a low-pass filtering effect for IPSCs would be beneficial because glutamatergic transmission also suffers from more rapid depression due to higher P_r. This aspect of on-demand disinhibition attributable to tonic anandamide-mediated changes will be further discussed below.

DISCUSSION

This study demonstrates that a decrease in anandamide tone, as a result of increased anandamide degradation, is responsible for synapse-specific adaptation of GABA release from CB1R-positive interneurons in the activity-deprived hippocampus (Supplementary Fig. 5). The reduced sizes of mIPSCs and uIPSCs (Fig. 1) meet the conventional compensatory homeostatic demand for weakened GABAergic synapses, and appear to occur at all GABAergic synapses detectable in pyramidal cell. However, a specific set of CB1R-positive, inhibitory synapses is selectively strengthened by an increase in basal P_r. Targeting

a specific subset of synapses is a critical step in maintaining complex circuits, and is accomplished by regulation of anandamide tone.

Anandamide as a tonically released endocannabinoid

Although 2-AG mediates major forms of endocannabinoid-dependent synaptic plasticity, such as DSI and GABAergic long-term depression in the hippocampus[10, 27, 33], the roles of endogenous anandamide in hippocampal synaptic regulation are largely unknown. Yet endogenous anandamide has often been implicated in behavioral roles, such as emotion[31] and learning[34]. The lack of evidence, however, at the cellular level for anandamide-mediated effects has created a major gap in understanding. Our data not only fill in the gap, but also indicate that the two endocannabinoids can be released from cells under different circumstances and are subject to different types of regulation.

N-acylphosphatidylethanolamine-hydrolyzing phospholipase D (NAPE-PLD), a widely-studied synthetic enzyme for anandamide[35], is located in axons and axon terminals, not in somata or dendrites, in hippocampal CA1[36–38]. Because our results (Fig. 3b) show that anandamide acts as a tonic retrograde messenger, it must be produced in the postsynaptic soma or dendrite. The apparent location of NAPE-PLD probably excludes it as the synthase of basal anandamide. Indeed, ablation of NAPE-PLD gene does not affect tonic levels of anandamide in the brain[39]. However, final exclusion of NAPE-PLD as a candidate synthase will depend on an unequivocal demonstration of its location (e.g., ref [36, 37] vs. ref [38]). The elucidation of the synthetic pathway for basal anandamide[35] will require localization of the enzymes involved and/or development of specific pharmacological tools. Some unique properties make anandamide seem especially appropriate for exerting tonic action on CB1R. First, anandamide is a partial agonist of CB1R, and is therefore less efficacious than full agonists[40, 41]. This property may allow other agonists with high efficacy such as 2-AG and WIN55212-2 to act in their full capacity, explaining why the WIN55212- 2 effects (Fig. 4) and DSI (Fig. 5) were unaltered. Second, anandamide desensitizes CB1R less than 2-AG does[40]. By minimizing constitutive desensitization, the endocannabinoid system can preserve the responsiveness to activity-dependent phasic stimulation. A lingering question is whether the amount of anandamide produced is also less in activity-deprived neurons. Our quantitative analysis based on the comparison of the actions of SR141716 and AM404 in control and chronic TTX tissue suggests that the total amount of anandamide tonically released is not greatly affected by activity deprivation (Supplementary Fig. 6). Nevertheless, direct investigation of this issue is required.

In contrast to the present result (Fig. 6d), we previously reported that URB597 had no effect on eIPSCs in acute hippocampal slices not preincubated with ω-agatoxin IVA[27]. This discrepancy could be attributed to the purity of the endocannabinoid bioassay: i.e., exclusion of CB1R-negative terminals with ω-agatoxin IVA. When we preincubated acute hippocampal slices with ω-agatoxin, 1 μM URB597 also suppressed eIPSC by 21 ± 5% (n = 5) (Supplementary Fig. 7). Hence, the mild anandamide tone and the basal role of FAAH are not culture-specific phenomena, but are present in more physiological, acute slices. The magnitude of the eIPSC increase (66%; Fig. 3a) caused by CB1R antagonist in the present study is larger than that reported with acute hippocampal slices (13%)[42]. The difference

might again be due to the use of ω-agatoxin. In fact, when CB1R-expressing presynaptic neurons are isolated by paired recording method, application of a CB1R antagonist can dramatically increase basal IPSC amplitude[25, 43]. Another possibility is that the higher temperature[42] may facilitate anandamide degradation, lowering its tone. However, we found that when control slice cultures were kept at 31 °C during recording, bath-applied SR141716 (2 μM) also increased the amplitude of eIPSC by 35 ± 9% (n = 5; Supplementary Fig. 8). This indicates that the tonic anandamide action is not an artifact of experimental conditions. Nevertheless, slice cultures are distinct from in vivo systems, hence the relevance of our study in living organism needs to be more carefully examined. In dissociated cultures of hippocampal neurons, tonic FAAH activity is absent and 2-AG is the dominant basal endocannabinoid[44]. This could be related to the immaturity of dissociated cultures, because the expression of FAAH in CA1 of rat hippocampus increases from postnatal day 8 to 22[45] and the basal anandamide level also rises with age[46]. Our slice cultures are more mature in terms of animal age at culturing and days in vitro than typical dissociated cultures.

Endocannabinoid tone as a major determinant of basal P_r

Our data suggest that, in activity-deprived neurons, the reduced tonic activation of CB1R is responsible for the enhanced basal P_r of CB1R-positive GABAergic synapses (Fig. 3e). Alternatively, it is conceivable that chronic TTX treatment increased the P_r independently of any changes in tonic endocannabinoid actions. If P_r of TTX-treated GABAergic synapses was already high, tonic CB1R activation would be less effective in suppressing release ("ceiling effect"), and SR141716 would therefore be less effective in enhancing it. To distinguish between a ceiling effect and a tonic endocannabinoid effect, we consider the critical prediction of the ceiling model: an increase in GABAergic P_r must decrease the ability of tonically released endocannabinoid to suppress eIPSCs[43, 47]. Therefore, the ceiling effect model predicts that the ability of CB1R activation to suppress eIPSCs will be decreased in TTX-treated cells.

We tested this prediction in two ways, with direct application of the CB1R agonist WIN55212-2, and by inducing phasic endocannabinoid actions with depolarization, i.e., DSI. The results of both tests (Figs. 4 and 5) are unambiguous: contrary to the predictions of the ceiling effect model, there is no change in DSI or the ability of WIN55212-2 to suppress eIPSCs. Therefore any underlying endocannabinoid-independent increase in P_r must have been insufficient to mask the inhibitory effects of CB1R activation. Because it fails this critical test, the ceiling effect model cannot account for our observations, and we conclude that the simplest explanation for the data remains the tonic endocannabinoid model.

Functional Significance

A homeostatic increase in network excitability often faces a challenge in balancing excitation and inhibition[2–4], especially when GABAergic synapses are globally scaled down. A way to control the risk might be to upregulate a sub-population and/or a certain property of GABAergic synapses, e.g., strengthening P_r of only a part of the interneuron population. This would help the system prevent the deleterious effects of widespread unchecked disinhibition. Indeed, our study suggests that the overall downregulation of inhibitory wiring, achieved by global decreases in IPSC amplitudes, may be partly

counterbalanced by increasing P_r of CB1R-positive synapses. It is therefore possible that CB1R-positive interneurons might play an important role in stabilizing the network during chronic inactivity.

Another advantage of increasing GABAergic P_r during chronic inactivity is that two opposite effects can be achieved: an increase in synaptic inhibition at low stimulation frequencies and greater short-term depression at high frequencies (≥20 Hz). The increased short-term depression turns the connection into a low-pass filter, because high frequency inhibitory transmission rapidly fades out. If inhibitory synaptic transmission depresses quickly during fast spiking, concomitant excitatory connections will be less shunted by GABA. Therefore, the net effect of elevated GABAergic P_r would favor excitation, consistent with homeostatic boosting of network gain, when circuits are repetitively activated[48].

Our study demonstrates that endocannabinoid tone is reduced by chronic inactivity and this phenomenon may be relevant to pathological situations, as modeled with deafferentation (Fig. 7). Damage to CA3 or lesions of Schaffer collaterals are often used as models for brain injury, as they induce changes like those of in vivo brain injury[49]. It is therefore possible to conjecture from our study that basal anandamide tone could be diminished following brain injury in vivo. In this case, a variety of cellular functions would be affected. Aforementioned contributions to circuit stabilization and synaptic integration seem to be favorable in terms of network homeostasis, but reduced anandamide tone could also have detrimental effects, given the various beneficial roles of endocannabinoids, such as neuroprotection[50]. For example, after brain injury, demand for endocannabinoid-mediated neuroprotection would be elevated, but an inactivity-induced decrease in endocannabinoid tone could prevent the demand from being met. In this case, the lowered tonic level of endocannabinoid would exacerbate the progress of neurodegeneration. A complete spectrum of endocannabinoid tone and its regulation by chronic activity levels should be further determined.

METHODS

Hippocampal Slices

Organotypic slice cultures were prepared from isolated hippocampi of 15 day old male Sprague-Dawley rats (Charles-River Laboratories, Wilmington, MA) that were isoflurane-anesthetized and decapitated. Slices (350 μm thick) were made with a vibrating slicer (Leica VT1200S; Wetzlar, Germany) in ice-cold saline consisting of (in mM) 123 NaCl, 3 KCl, 26 $NaHCO_3$, 1 NaH_2PO_4, 0.7 $CaCl_2$, 3.3 $MgSO_4$, 15 glucose (300–305 mOsm), bubbled with 95% O_2/5% CO_2. After washing the slices with culture medium (37 °C), we placed them on culture membranes (Millipore, Billerica, MA) at the interface of culture medium and air at 37 °C. The medium was exchanged every 2–3 days, and was composed of 50% Basal Medium Eagle, 25% Earle's salt solution, 25% horse serum, 2 mM L-glutamine and 10 mM HEPES, supplemented with 5 mM glucose. Acute slices of hippocampus used in Supplementary Figure 7 were 400μm thick and were obtained from 4–6 week old Sprague-Dawley rats. The acute slices were kept at the interface of 95% O_2/5% CO_2 and bath solution (see below for composition) at 22–24 °C. The protocols were approved by the Institutional Animal Care and Use Committee of University of Maryland.

Electrophysiology

Recordings were made from slice cultures at 18–22 days in vitro (DIV). To chronically suppress neuronal firing, we exposed slices to 1 μM TTX for 3–5 days, starting as early as 15 DIV. Slices were removed from TTX-containing media for 30–60 min before starting recording. Control slices were not treated with TTX. When CA3 or subiculum was removed from slice cultures (Fig. 7), the microsurgery was done at 15–18 DIV and recordings were made 5–7 days later. Whole-cell voltage clamp recordings from CA1 pyramidal neurons (one cell per slice) were carried out at 22–24 °C while the recording chamber was perfused with bath solution at ~1.5 ml/min. Only in the experiment in Supplementary Figure 8, was the temperature of bath solution warmed to 31 ± 0.5 °C. The bath solution contained (in mM) 123 NaCl, 3 KCl, 26 $NaHCO_3$, 1 NaH_2PO_4, 2.5 $CaCl_2$, 1.5 $MgSO_4$, 15 glucose (300–305 mOsm) and was equilibrated with 95% O_2/5% CO_2. Electrode resistance in the bath solution was 3–4 MΩ and series resistance (<25 MΩ) was stable within 15%. Data were collected using Axopatch 200B (Molecular Devices, Sunnyvale, CA), filtered at 1 kHz and digitized at 50 kHz using a Digidata 1322A and the Clampex 9 program (Molecular Devices). The pipette solution for recordings of mIPSC, uIPSC (Fig. 1) and sIPSC (Fig. 2a–c) contained (in mM) 135 KCl, 2 NaCl, 1 $MgSO_4$, 0.2 $CaCl_2$, 2 EGTA, 5 QX314-Cl, 4 ATP-Mg, 0.3 GTP-tris and 10 HEPES (pH = 7.2 with KOH, 290–295 mOsm with sucrose). The "zero-Ca^{2+}" pipette solution (Figs. 3b and 6h) was made with (in mM) 146 K-gluconate, 1.4 NaCl, 1 $MgSO_4$, 1.8 EGTA, 4 ATP-Mg, 0.3 GTP-tris and 10 HEPES (pH = 7.2 with KOH, 290–295 mOsm). The free [Ca^{2+}] of this solution is 1.0 nM when calculated with MaxChelator (http://www.stanford.edu/~cpatton/maxc.html) assuming pure water is contaminated with 10 μM Ca^{2+}. The free [EGTA] is also calculated to be 1.7 mM. In all other experiments, we used a pipette solution containing (in mM) 146 K-gluconate, 1 NaCl, 1 $MgSO_4$, 0.2 $CaCl_2$, 2 EGTA, 4 ATP-Mg, 0.3 GTP-tris and 10 HEPES (pH = 7.2 with KOH, 290–295 mOsm). This "normal" pipette solution contained 19.7 nM free [Ca^{2+}] and 1.7 mM free [EGTA] as calculated by MaxChelator.

All voltage clamp recordings were made at a holding potential of −65 mV. mIPSCs were recorded in NBQX (10 μM), D-AP5 (40 μM) and TTX (0.5 μM). eIPSCs were measured in NBQX (10 μM) and D-AP5 (40 μM). EPSCs were recorded in the presence of 10 μM gabazine and 40 μM D-AP5 along with 0.3 μM NBQX for prevention of polysynaptic excitation. Evoked synaptic currents were elicited by a stimulus delivered through a monopolar glass electrode filled with the bath solution (~1 MΩ resistance) and located in CA1 stratum pyramidale for eIPSCs or CA1 stratum radiatum for eEPSCs. Presynaptic cells were stimulated every 12 s, except for DSI measurements where a 6-s interval was used.

Vehicle for SR141716, AM251, WIN55212-2, URB597, anandamide and capsazepine was 0.01% (v/v) ethanol, which by itself had no effect on eIPSC amplitude (98 ± 2% of baseline at 15–21 min of ethanol; n = 5; $P > 0.7$, paired t-test) (data not shown). In experiments where AM404 was bath-applied, the vehicle (0.02% ethanol) was already present in the bath solution during the baseline period before AM404 application. The stock solutions of ω-agatoxin IVA and URB597 were kept for up to 2 months and 2 weeks, respectively. TTX, gabazine, WIN55212-2, ω-conotoxin GVIA and capsazepine were purchased from Tocris (Ellisville, MO), and NBQX, D-AP5 and AM404 were from Ascent Scientific (Bristol, UK).

Anandamide (as a 144-mM stock solution), AM251 and URB597 were obtained from Cayman Chemical (Ann Arbor, MI) and ω-agatoxin IVA was obtained from Peptide International (Louisville, KY). SR141716 was provided by the National Institute on Drug Abuse drug supply service (Research Triangle Park, NC). Other chemicals were from Sigma (St. Louis, MO).

Ca^{2+} imaging

For imaging pyramidal cell $[Ca^{2+}]$, 200 μM Fura-2 was included in the pipette solution. The data were acquired >20 min after establishing a whole-cell recording to allow for sufficient dialysis with the indicator. Fura-2 was excited by alternating illumination of 340 and 380 nm wavelength light from a Lambda DG-4 lamp (Sutter Instrument, Novato, CA). The emitted fluorescence from the indicator was passed through a 510 nm filter and detected with a Cascade CCD camera (Roper Scientific, Tucson, AZ). Pairs of images with 340 and 380 nm illumination were obtained at 1 Hz. An average of 20–30 “dark noise” images, which were obtained at the end of each experiment with the illumination shutter closed, was subtracted from experimental images. The mean background fluorescence of an area outside the dialyzed cell was also subtracted from the mean somatic fluorescence. Raw images were acquired with MetaFluor software (Molecular Devices, Downingtown, PA) and analyzed offline with MetaFluor Analyst program (Molecular Devices). The ratio of fluorescence (R) was calculated by dividing fluorescence at 340 nm (F_{340}) by F_{380} (i.e., $R = F_{340}/F_{380}$). The Ca^{2+} concentration was estimated with the following equation: $[Ca^{2+}] = K_D \cdot (F_{380,min}/F_{380,max}) \cdot [(R - R_{min})/(R_{max} - R)]$, where K_D for Fura-2 is 140 nM, the subscript “min” means a value obtained in a Ca^{2+}-free condition, and the subscript “max” means a saturating Ca^{2+} condition. The F_{min} was acquired by measuring somatic $[Ca^{2+}]_{in}$ in four cells with a pipette solution containing (in mM) 112 K-gluconate, 2 NaCl, 15 EGTA, 30 HEPES and 0.2 Fura-2 (pH = 7.2). The F_{max} was measured from four cells with a pipette solution composed of (in mM) 138 K-gluconate, 1 NaCl, 10 $CaCl_2$, 10 HEPES and 0.2 Fura-2 (pH = 7.2). R_{min} is the ratio of fluorescence, 340 nm to 380 nm, measured with the Ca^{2+}-free calibrating solution used for measuring F_{min} (see above) (i.e., $R_{min} = F_{340,min}/F_{380,min}$). R_{max} is the ratio of F_{340}/F_{380} with the high-Ca^{2+} calibrating solution (see above) (i.e., $R_{max} = F_{340,max}/F_{380,max}$). Cells were depolarized from −65 mV to 0 mV for 500 ms every 3 min and $[Ca^{2+}]_{in}$ responses to 2–3 depolarization trials for a given cell were averaged. The basal $[Ca^{2+}]_{in}$ was averaged for 23 s before each depolarization and peak $[Ca^{2+}]_{in}$ after depolarization was averaged for 5 s starting from the maximal $[Ca^{2+}]_{in}$. We confirmed that Fura-2 was not saturated by Ca with the 500 ms depolarizations because 5 s depolarizations induced higher rises in $[Ca^{2+}]_{in}$ (saturating, supra-μM range) in every cell (data not shown).

Data analysis

Individual mIPSCs and sIPSCs were detected using Clampfit software (Molecular Devices) with a template match threshold of 7. The template trace, made from our own data, was 9 ms long, including a 3 ms baseline. We used the short template window to detect mainly the IPSC rising phase with a small portion of the decay phase, thus catching most of the partially overlapped events at a cost of decay time information. Mean amplitude and mean frequency of mIPSCs were calculated from 500 events per cell and mean values were subjected to t-tests. sIPSCs were collected from recordings of which the mean length was

266 ± 12 s. For minimal stimulation that evoked uIPSCs (Fig. 1c–**e**), stimulation started from an intensity where all the stimulations failed to evoke an IPSC. As the intensity was gradually increased, uIPSCs with a relatively constant amplitude were evoked with a success ratio increasing with intensity up to a maximum. Because the success ratio varied with stimulus intensity, the ratio did not faithfully reflect the P_r of the nerve terminal, thus precluding the use of the "method of failures" to analyze transmission. Failures were omitted when calculating uIPSC amplitudes.

The scaling of mIPSCs (Fig. 1b) was performed as reported[18, 19]: we plotted the rank-ordered TTX-treated amplitudes against the rank-ordered control amplitudes, and fitted the plot with a straight line. Because non-uniform distribution of extreme amplitudes tends to distort the rank-order plot, the fitting was made with mIPSCs only in the 10–90th percentile of amplitudes. The fitted line generated a slope of 0.590 and an intercept of 5.03 (R^2 = 0.999). All control mIPSCs were then scaled down using these values. The peak amplitudes of evoked synaptic currents were measured over a 0.5-ms window from individual traces, and then the peak values of 20–50 traces were averaged for a given condition per cell. To determine the ratio of short-term depression or facilitation, the mean amplitudes of the second or third responses in the 20 Hz train were normalized to the mean of the first currents. Stimulus artifacts were graphically truncated in the figures for clarity.

DSI, as a cumulative suppression eIPSCs, was quantified by integrating percentage suppression of eIPSC amplitudes over 6–144 s (for 500 ms depolarization) or 0–240 s (for 5 s depolarization). For example, if eIPSCs after depolarization were completely reduced (i.e., by 100%) for >4 min, the DSI magnitude would be 13,800 %·s (100% × 138 s) for 500 ms depolarization or 24,000 %·s for 5 s depolarization. Cells were depolarized every 3 min when 500-ms depolarizations were used and every 5 min when 5-s pulses were used. For a given cell, 2–3 DSI trials were averaged except for the AM404 experiments (Fig. 6b). In the presence of AM404, only one (the first) DSI trial was sampled to avoid occlusion of DSI by accumulated 2-AG. AM404 was applied for >25 min without any depolarization and then cells were depolarized once for 5 s. In the experiments on DSI with 500 ms depolarization, 200 μM Fura-2 was always present in the pipette solution for simultaneous imaging of intracellular [Ca^{2+}]. Therefore, DSI was measured >20 min after establishing a whole-cell mode to allow for sufficient dialysis with Fura-2. For DSI with 5 s depolarization, only 50% of the cells had Fura-2 in the pipette. Since DSI magnitude was not significantly different in the absence and presence of Fura-2 ($P > 0.3$, t-test between Fura-2 and non-Fura-2, separately for control and TTX-treated cells), the data were pooled. In the 5-s DSI experiments, DSI was also measured >20 min after breaking the membrane regardless of the presence of Fura-2. When drugs were applied to the bath solution, eIPSC amplitudes were sampled when the changes reached a steady state: 12–16 min after the onset of SR141716, 17–22 min after AM404, 20–25 min after URB597 and 12–15 after anandamide.

Comparisons between two independent groups were made using t-tests with a two-tailed confidence level of $P < 0.05$, and a paired t-test was employed to determine changes within a cell (e.g., before and after a drug). Multiple comparisons (Figs. 2d,**e**, 7b and 8c) were performed with two-way ANOVA: if the ANOVA revealed a significant difference ($P < 0.05$) between control and treated groups, Bonferroni t-tests were used for pairwise

comparisons between control and treated cells within each I/EPSC number. All data represent mean ± s.e.m.

Supplementary Material

Refer to Web version on PubMed Central for supplementary material.

Acknowledgments

We thank Dr. Thomas Abrams and the members of the Alger lab for helpful comments and suggestions on this work. We thank Dr. Tony Gover for expert assistance with the calcium imaging experiments. This research was supported by NIH grant R01 DA014625 and R01 MH077277 to B.E.A.

References

1. Turrigiano GG. The self-tuning neuron: synaptic scaling of excitatory synapses. Cell. 2008; 135:422–435. [PubMed: 18984155]
2. Houweling AR, Bazhenov M, Timofeev I, Steriade M, Sejnowski TJ. Homeostatic synaptic plasticity can explain post-traumatic epileptogenesis in chronically isolated neocortex. Cereb Cortex. 2005; 15:834–845. [PubMed: 15483049]
3. Trasande CA, Ramirez JM. Activity deprivation leads to seizures in hippocampal slice cultures: is epilepsy the consequence of homeostatic plasticity? J Clin Neurophysiol. 2007; 24:154–164. [PubMed: 17414971]
4. Kim J, Tsien RW. Synapse-specific adaptations to inactivity in hippocampal circuits achieve homeostatic gain control while dampening network reverberation. Neuron. 2008; 58:925–937. [PubMed: 18579082]
5. Bausch SB, He S, Petrova Y, Wang XM, McNamara JO. Plasticity of both excitatory and inhibitory synapses is associated with seizures induced by removal of chronic blockade of activity in cultured hippocampus. J Neurophysiol. 2006; 96:2151–2167. [PubMed: 16790597]
6. Buckby LE, Jensen TP, Smith PJ, Empson RM. Network stability through homeostatic scaling of excitatory and inhibitory synapses following inactivity in CA3 of rat organotypic hippocampal slice cultures. Mol Cell Neurosci. 2006; 31:805–816. [PubMed: 16500111]
7. Echegoyen J, Neu A, Graber KD, Soltesz I. Homeostatic plasticity studied using in vivo hippocampal activity-blockade: synaptic scaling, intrinsic plasticity and age-dependence. PLoS ONE. 2007; 2:e700. [PubMed: 17684547]
8. Burrone J, Murthy VN. Synaptic gain control and homeostasis. Curr Opin Neurobiol. 2003; 13:560–567. [PubMed: 14630218]
9. Alger BE. Retrograde signaling in the regulation of synaptic transmission: focus on endocannabinoids. Prog Neurobiol. 2002; 68:247–286. [PubMed: 12498988]
10. Kano M, Ohno-Shosaku T, Hashimotodani Y, Uchigashima M, Watanabe M. Endocannabinoid-mediated control of synaptic transmission. Physiol Rev. 2009; 89:309–380. [PubMed: 19126760]
11. Katona I, et al. Presynaptically located CB1 cannabinoid receptors regulate GABA release from axon terminals of specific hippocampal interneurons. J Neurosci. 1999; 19:4544–4558. [PubMed: 10341254]
12. Marsicano G, Lutz B. Expression of the cannabinoid receptor CB1 in distinct neuronal subpopulations in the adult mouse forebrain. Eur J Neurosci. 1999; 11:4213–4225. [PubMed: 10594647]
13. Chen K, et al. Long-term plasticity of endocannabinoid signaling induced by developmental febrile seizures. Neuron. 2003; 39:599–611. [PubMed: 12925275]
14. Falenski KW, Blair RE, Sim-Selley LJ, Martin BR, DeLorenzo RJ. Status epilepticus causes a long-lasting redistribution of hippocampal cannabinoid type 1 receptor expression and function in the rat pilocarpine model of acquired epilepsy. Neuroscience. 2007; 146:1232–1244. [PubMed: 17433556]

15. Rinaldi-Carmona M, et al. Modulation of CB1 cannabinoid receptor functions after a long-term exposure to agonist or inverse agonist in the Chinese hamster ovary cell expression system. J Pharmacol Exp Ther. 1998; 287:1038–1047. [PubMed: 9864290]
16. Hsieh C, Brown S, Derleth C, Mackie K. Internalization and recycling of the CB1 cannabinoid receptor. J Neurochem. 1999; 73:493–501. [PubMed: 10428044]
17. Hartman KN, Pal SK, Burrone J, Murthy VN. Activity-dependent regulation of inhibitory synaptic transmission in hippocampal neurons. Nat Neurosci. 2006; 9:642–649. [PubMed: 16582905]
18. Kilman V, van Rossum MC, Turrigiano GG. Activity deprivation reduces miniature IPSC amplitude by decreasing the number of postsynaptic $GABA_A$ receptors clustered at neocortical synapses. J Neurosci. 2002; 22:1328–1337. [PubMed: 11850460]
19. Turrigiano GG, Leslie KR, Desai NS, Rutherford LC, Nelson SB. Activity-dependent scaling of quantal amplitude in neocortical neurons. Nature. 1998; 391:892–896. [PubMed: 9495341]
20. Bertrand S, Lacaille JC. Unitary synaptic currents between lacunosum-moleculare interneurones and pyramidal cells in rat hippocampus. J Physiol. 2001; 532:369–384. [PubMed: 11306657]
21. Bartley AF, Huang ZJ, Huber KM, Gibson JR. Differential activity-dependent, homeostatic plasticity of two neocortical inhibitory circuits. J Neurophysiol. 2008; 100:1983–1994. [PubMed: 18701752]
22. Maffei A, Nelson SB, Turrigiano GG. Selective reconfiguration of layer 4 visual cortical circuitry by visual deprivation. Nat Neurosci. 2004; 7:1353–1359. [PubMed: 15543139]
23. Poncer JC, McKinney RA, Gahwiler BH, Thompson SM. Either N- or P-type calcium channels mediate GABA release at distinct hippocampal inhibitory synapses. Neuron. 1997; 18:463–472. [PubMed: 9115739]
24. Wilson RI, Kunos G, Nicoll RA. Presynaptic specificity of endocannabinoid signaling in the hippocampus. Neuron. 2001; 31:453–462. [PubMed: 11516401]
25. Neu A, Foldy C, Soltesz I. Postsynaptic origin of CB1-dependent tonic inhibition of GABA release at cholecystokinin-positive basket cell to pyramidal cell synapses in the CA1 region of the rat hippocampus. J Physiol. 2007; 578:233–247. [PubMed: 17053036]
26. Faber DS, Korn H. Applicability of the coefficient of variation method for analyzing synaptic plasticity. Biophys J. 1991; 60:1288–1294. [PubMed: 1684726]
27. Kim J, Alger BE. Inhibition of cyclooxygenase-2 potentiates retrograde endocannabinoid effects in hippocampus. Nat Neurosci. 2004; 7:697–698. [PubMed: 15184902]
28. Makara JK, et al. Selective inhibition of 2-AG hydrolysis enhances endocannabinoid signaling in hippocampus. Nat Neurosci. 2005; 8:1139–1141. [PubMed: 16116451]
29. Fortin DA, Trettel J, Levine ES. Brief trains of action potentials enhance pyramidal neuron excitability via endocannabinoid-mediated suppression of inhibition. J Neurophysiol. 2004; 92:2105–2112. [PubMed: 15175370]
30. Giuffrida A, Beltramo M, Piomelli D. Mechanisms of endocannabinoid inactivation: biochemistry and pharmacology. J Pharmacol Exp Ther. 2001; 298:7–14. [PubMed: 11408519]
31. Piomelli D, et al. Pharmacological profile of the selective FAAH inhibitor KDS-4103 (URB597). CNS Drug Rev. 2006; 12:21–38. [PubMed: 16834756]
32. Kawamura Y, et al. The CB1 cannabinoid receptor is the major cannabinoid receptor at excitatory presynaptic sites in the hippocampus and cerebellum. J Neurosci. 2006; 26:2991–3001. [PubMed: 16540577]
33. Chevaleyre V, Castillo PE. Heterosynaptic LTD of hippocampal GABAergic synapses: a novel role of endocannabinoids in regulating excitability. Neuron. 2003; 38:461–472. [PubMed: 12741992]
34. Varvel SA, Wise LE, Niyuhire F, Cravatt BF, Lichtman AH. Inhibition of fatty-acid amide hydrolase accelerates acquisition and extinction rates in a spatial memory task. Neuropsychopharmacology. 2007; 32:1032–1041. [PubMed: 17047668]
35. Okamoto Y, Wang J, Morishita J, Ueda N. Biosynthetic pathways of the endocannabinoid anandamide. Chem Biodivers. 2007; 4:1842–1857. [PubMed: 17712822]
36. Nyilas R, et al. Enzymatic machinery for endocannabinoid biosynthesis associated with calcium stores in glutamatergic axon terminals. J Neurosci. 2008; 28:1058–1063. [PubMed: 18234884]

37. Egertova M, Simon GM, Cravatt BF, Elphick MR. Localization of N-acyl phosphatidylethanolamine phospholipase D (NAPE-PLD) expression in mouse brain: A new perspective on N-acylethanolamines as neural signaling molecules. J Comp Neurol. 2008; 506:604–615. [PubMed: 18067139]

38. Cristino L, et al. Immunohistochemical localization of anabolic and catabolic enzymes for anandamide and other putative endovanilloids in the hippocampus and cerebellar cortex of the mouse brain. Neuroscience. 2008; 151:955–968. [PubMed: 18248904]

39. Leung D, Saghatelian A, Simon GM, Cravatt BF. Inactivation of N-acyl phosphatidylethanolamine phospholipase D reveals multiple mechanisms for the biosynthesis of endocannabinoids. Biochemistry. 2006; 45:4720–4726. [PubMed: 16605240]

40. Luk T, et al. Identification of a potent and highly efficacious, yet slowly desensitizing CB1 cannabinoid receptor agonist. Br J Pharmacol. 2004; 142:495–500. [PubMed: 15148260]

41. Sugiura T. Physiological roles of 2-arachidonoylglycerol, an endogenous cannabinoid receptor ligand. Biofactors. 2009; 35:88–97. [PubMed: 19319851]

42. Kim J, Isokawa M, Ledent C, Alger BE. Activation of muscarinic acetylcholine receptors enhances the release of endogenous cannabinoids in the hippocampus. J Neurosci. 2002; 22:10182–10191. [PubMed: 12451119]

43. Losonczy A, Biro AA, Nusser Z. Persistently active cannabinoid receptors mute a subpopulation of hippocampal interneurons. Proc Natl Acad Sci U S A. 2004; 101:1362–1367. [PubMed: 14734812]

44. Hashimotodani Y, Ohno-Shosaku T, Kano M. Presynaptic monoacylglycerol lipase activity determines basal endocannabinoid tone and terminates retrograde endocannabinoid signaling in the hippocampus. J Neurosci. 2007; 27:1211–1219. [PubMed: 17267577]

45. Morozov YM, Ben-Ari Y, Freund TF. The spatial and temporal pattern of fatty acid amide hydrolase expression in rat hippocampus during postnatal development. Eur J Neurosci. 2004; 20:459–466. [PubMed: 15233754]

46. Fernandez-Ruiz J, Berrendero F, Hernandez ML, Ramos JA. The endogenous cannabinoid system and brain development. Trends Neurosci. 2000; 23:14–20. [PubMed: 10631784]

47. Foldy C, Neu A, Jones MV, Soltesz I. Presynaptic, activity-dependent modulation of cannabinoid type 1 receptor-mediated inhibition of GABA release. J Neurosci. 2006; 26:1465–1469. [PubMed: 16452670]

48. Glickfeld LL, Scanziani M. Distinct timing in the activity of cannabinoid-sensitive and cannabinoid-insensitive basket cells. Nat Neurosci. 2006; 9:807–815. [PubMed: 16648849]

49. McKinney RA, Debanne D, Gahwiler BH, Thompson SM. Lesion-induced axonal sprouting and hyperexcitability in the hippocampus in vitro: implications for the genesis of posttraumatic epilepsy. Nat Med. 1997; 3:990–996. [PubMed: 9288725]

50. van der Stelt M, Di Marzo V. Cannabinoid receptors and their role in neuroprotection. Neuromolecular Med. 2005; 7:37–50. [PubMed: 16052037]

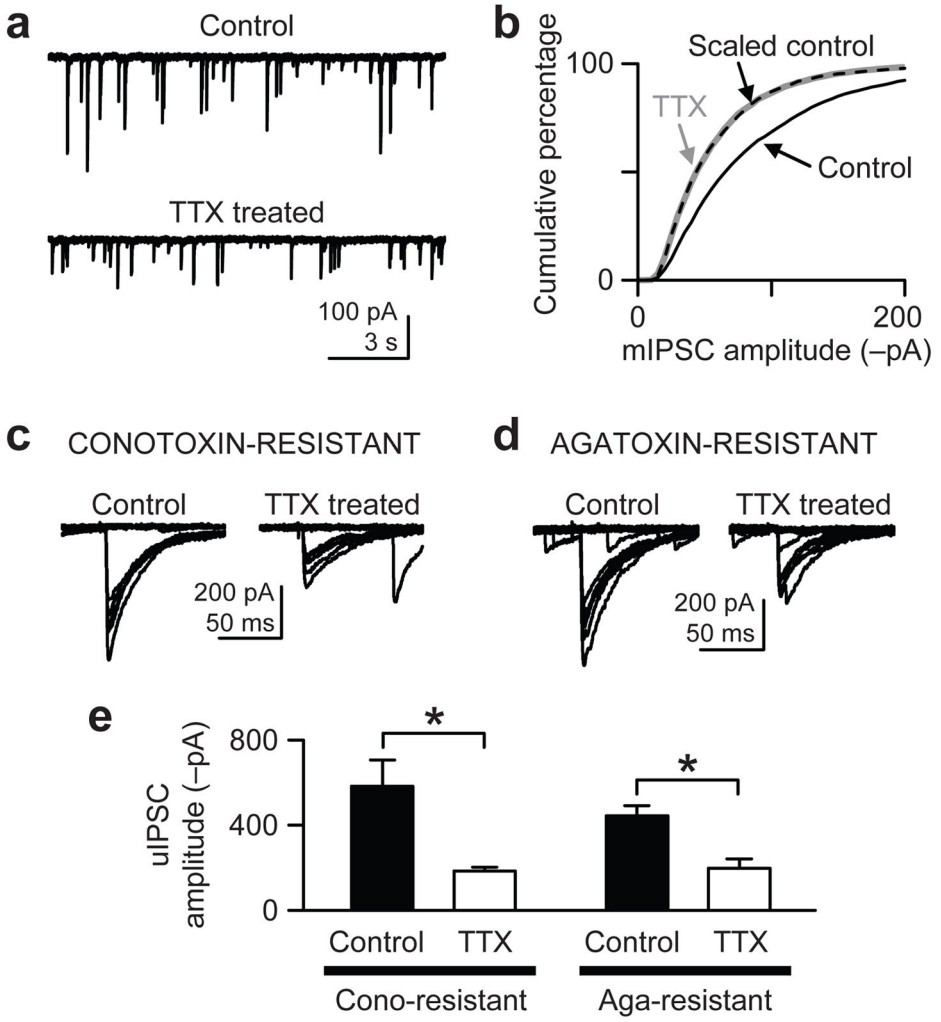

Figure 1.

Homeostatic downregulation of inhibitory synapses caused by chronic TTX treatment. (**a**) Whole-cell recordings of mIPSCs from CA1 pyramidal neurons in control and TTX-treated (3–5 days) slice cultures of rat hippocampus. Cells were voltage-clamped at −65 mV with a pipette solution containing 142.4 mM Cl^-. (**b**) Cumulative distributions of mIPSCs (500 events per cell) show that chronic TTX reduced mIPSC amplitudes. The distribution of the scaled control data (dashed line), obtained after scaling down individual mIPSCs (see Methods), essentially overlapped exactly with the TTX-treated mIPSC distribution (thick gray line) ($P > 0.9$, Kolmogorov-Smirnov test between *TTX* and *Scaled control*), suggesting a global scaling of mIPSCs. (**c**) uIPSCs were evoked by extracellular minimal stimulation. Stimulus intensity was gradually increased until uIPSCs were elicited in an all-or-none fashion and consistently occurred, as shown in the sample traces. Slice cultures were preincubated with 500 nM ω-conotoxin GVIA for 15–30 min just before recording to isolate synapses that use P/Q-type Ca^{2+} channels for GABA release. (**d**) Same experiment as in **c**, but the slice cultures were preincubated with 300 nM ω-agatoxin IVA for 15–30 min. (**e**) Group data of uIPSC amplitudes show the mean amplitudes were reduced by chronic TTX

in both conotoxin- and agatoxin-resistant synapses. *, $P < 0.02$. Error bars represent s.e.m. in this and all other figures.

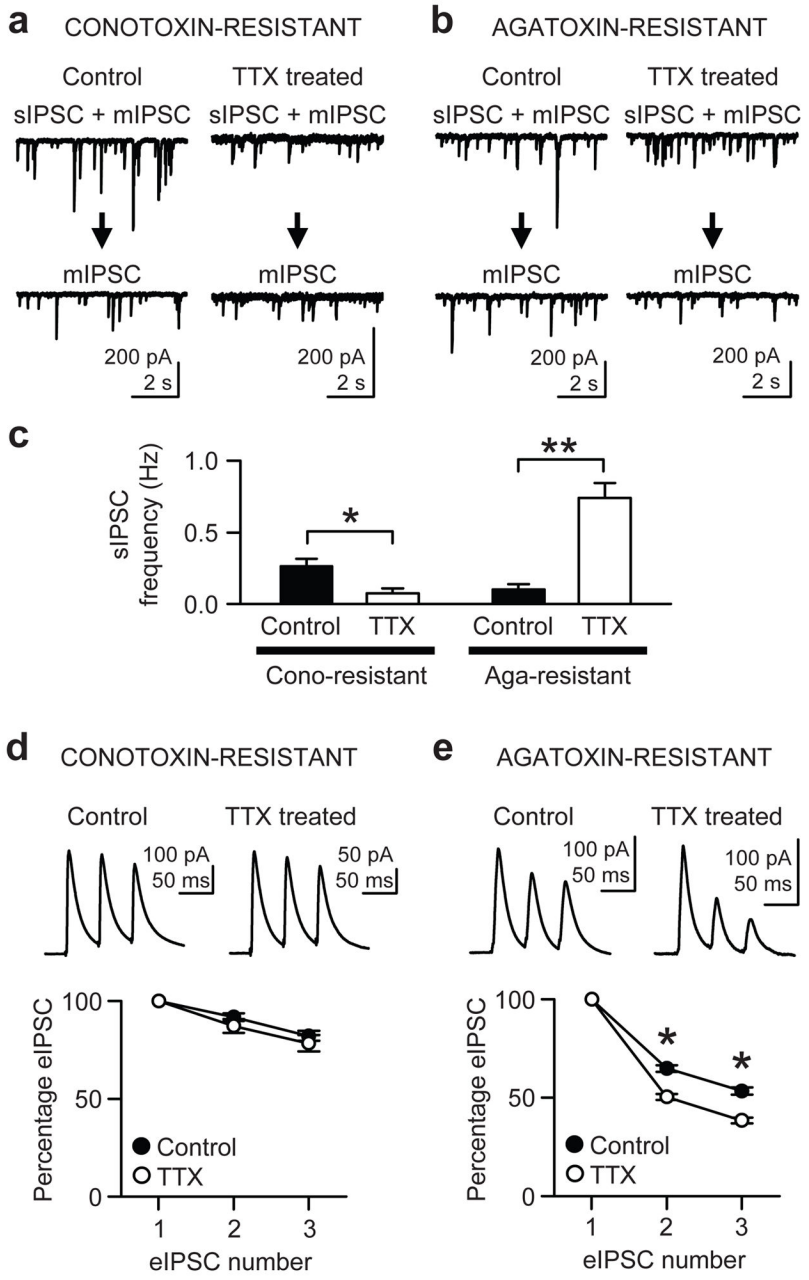

Figure 2.

Inactivity-induced upregulation of synaptic properties in a subset of inhibitory interneurons. (**a**) sIPSCs were recorded at −65 mV with 142.4 mM Cl^- in the pipette solution. In each cell, first a mixture of sIPSCs and mIPSCs was recorded and then, after addition of 0.5 μM TTX, only mIPSCs were obtained. sIPSC frequency was found by subtracting the frequency of mIPSCs from the total of sIPSCs + mIPSCs in the same cell. Slice cultures were preincubated in 500 nM ω-conotoxin GVIA for 15–30 min. (**b**) Same experiment as in **a**, but the cultures were preincubated with 300 nM ω-agatoxin IVA for 15–30 min. (**c**) Group data of sIPSC frequency. *, $P < 0.02$. **, $P < 0.0005$. (**d**) Short-term plasticity of eIPSCs was

examined with extracellular stimulation of presynaptic axons at 20 Hz. In this and all subsequent experiments, pipette [Cl^-] was lowered to 1.4 mM, which kept eIPSC amplitudes small and preserved adequate voltage clamp control. Slice cultures were preincubated with ω-conotoxin GVIA for 15–30 min. Amplitudes of the second and the third eIPSCs were normalized to the first eIPSCs. No difference was found between control and TTX-treated cells in short-term depression of eIPSCs from P/Q-type Ca^{2+} channel-containing terminals ($P > 0.2$). (**e**) Short-term depression of eIPSCs from terminals with N-type Ca^{2+} channels was measured after preincubation with ω-agatoxin IVA for 15–30 min. TTX-treated cells showed more pronounced depression, suggesting an increase in P_r. *, $P < 0.001$.

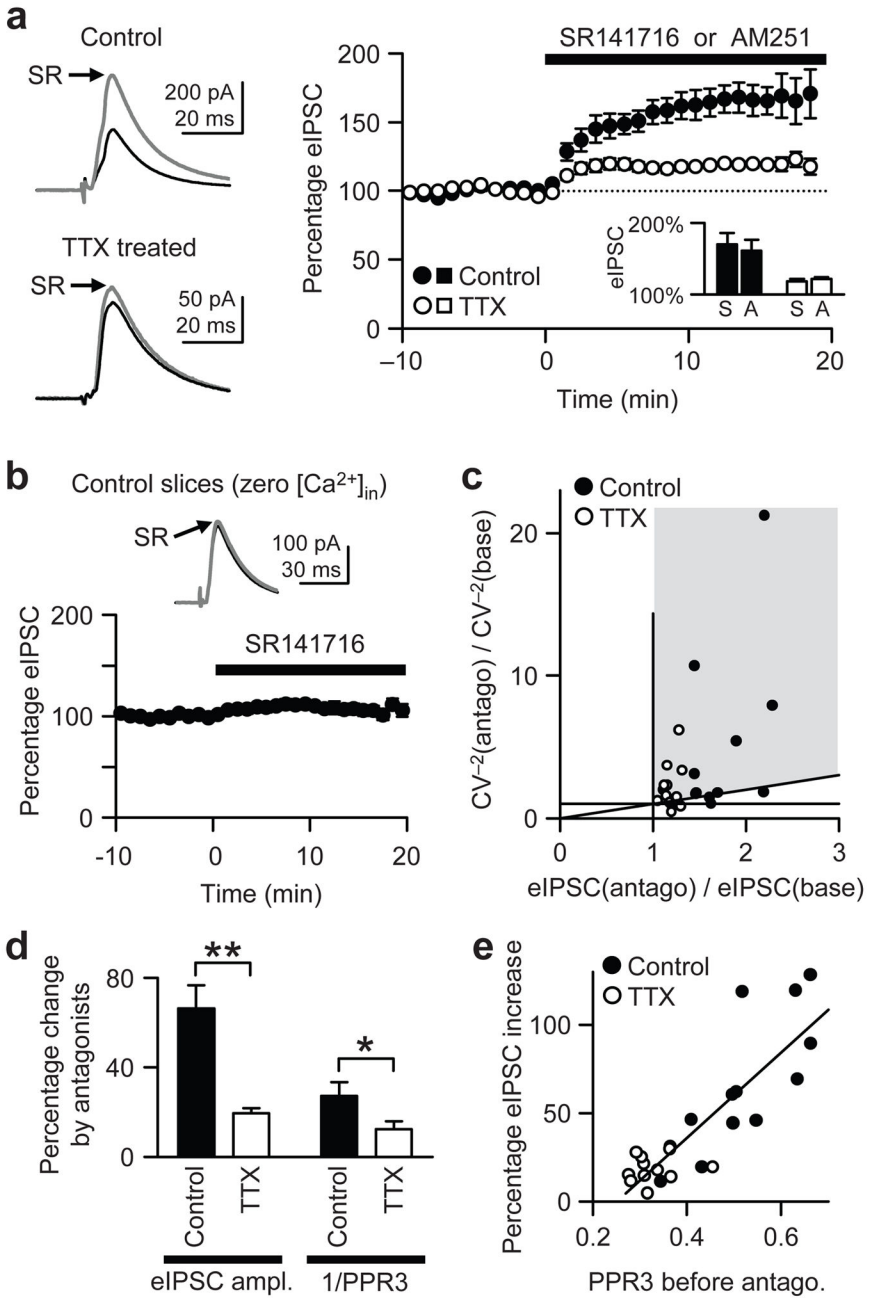

Figure 3.

Tonic activation of CB1R is reduced by activity deprivation. (**a**) Mean amplitude of agatoxin-resistant eIPSCs was enhanced by a CB1R antagonist, either SR141716 (2 μM) or AM251 (2 μM). Black traces, averaged eIPSCs before SR141716; gray traces, averaged eIPSCs in SR141716. In the right graph, eIPSC amplitudes were normalized to baseline values before SR141716. Inset, effects of SR141716 (*S*) were not significantly different from those of AM251 (*A*) in either control or TTX groups ($P > 0.5$). (**b**) SR141716 (2 μM) failed to increase eIPSCs in control slices when a zero-Ca^{2+} pipette solution was used for recording. (**c**) From the data in **a**, the ratio of CV^{-2} in CB1R antagonist to baseline CV^{-2}

[CV^{-2}(antago)/CV^{-2}(base)] is plotted against the ratio of eIPSC amplitudes in CB1R antagonist to baseline values [eIPSC(antago)/eIPSC(base)]. Data points in gray area and along the diagonal line of $y = x$ imply a presynaptic enhancement of transmission caused by either SR147161 or AM251. (**d**) The larger increase in eIPSC caused by CB1R antagonists in control cells than in TTX-treated cells, is accompanied by a larger increase in $PPR3^{-1}$, which is proportional to P_r. Data in **a** were analyzed. *, $P < 0.05$. **, $P < 0.01$. (**e**) The eIPSC increase induced by a CB1R antagonist is plotted against PPR3 before the antagonist. When PPR3 was high (low basal P_r), the eIPSC increase was larger. Straight line is a linear fit with square of correlation coefficient (R^2) of 0.71.

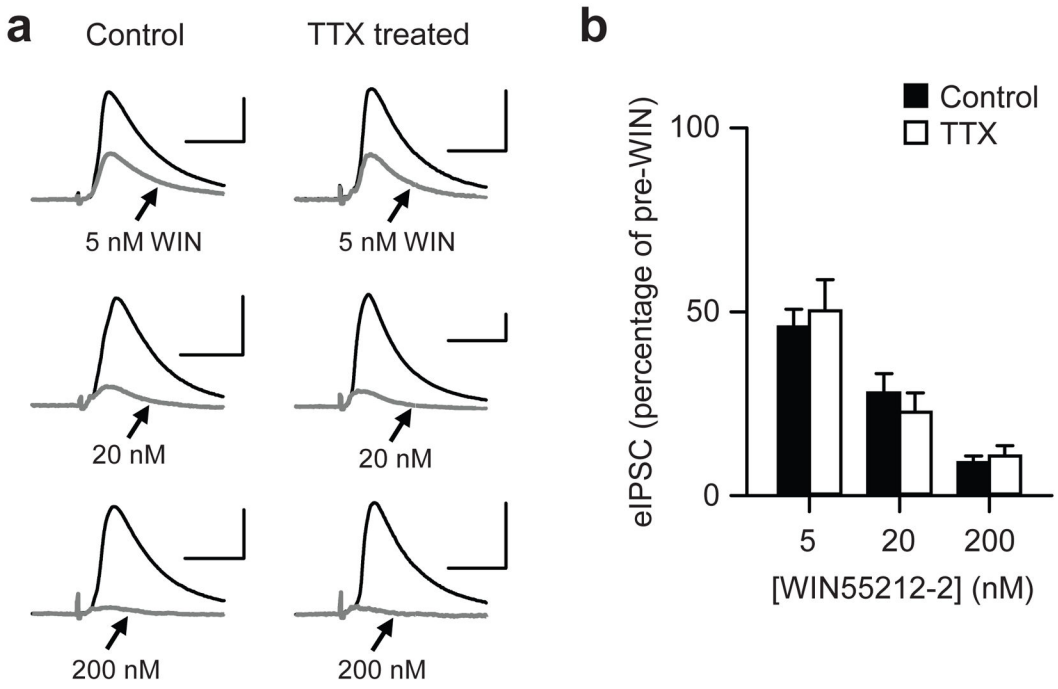

Figure 4.

Chronic inactivity does not alter the responsiveness of CB1R to WIN55212-2, a CB1R agonist. (**a**) Representative traces of agatoxin-resistant eIPSCs from three control and three TTX-treated cells at different concentrations of WIN55212-2 (5, 20, and 200 nM). Black, average of baseline eIPSCs before WIN55212-2; gray, average of steady-state eIPSCs in the presence of WIN55212-2. All scale bars, 100 pA and 20 ms. (**b**) eIPSC amplitudes in the presence of WIN55212-2 were normalized to the pre-WIN55212-2 baseline. No significant difference was found between the responses of control and TTX-treated cells at any concentration ($P > 0.4$).

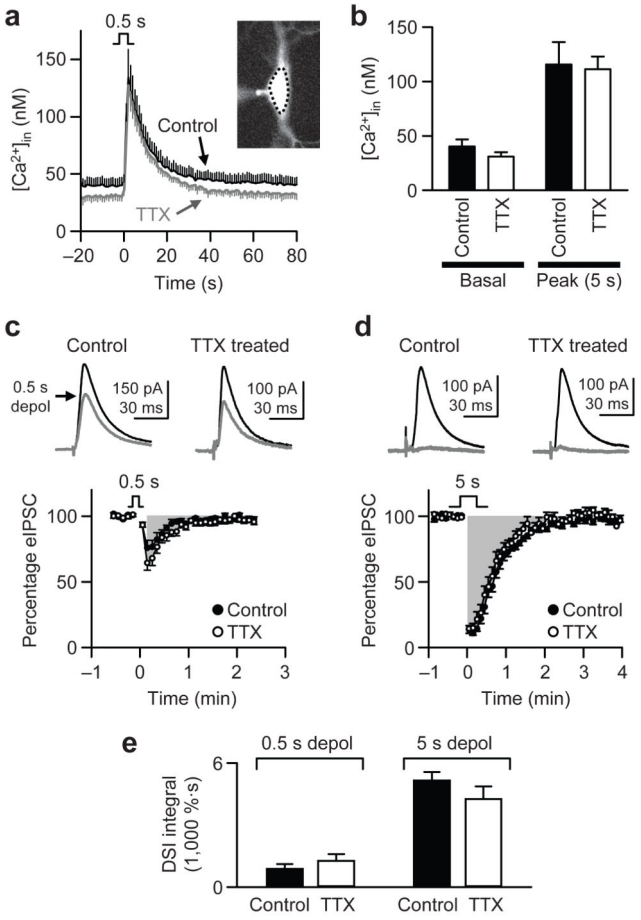

Figure 5.

Basal $[Ca^{2+}]_{in}$ and Ca^{2+}-dependent 2-AG release are not affected by chronic TTX. Slice cultures were preincubated with 300 nM ω-agatoxin IVA for 15–30 min. (**a**) Somatic $[Ca^{2+}]_{in}$ in postsynaptic cells was imaged at 1 Hz with 200 μM Fura-2 in the pipette solution. Pyramidal cells were depolarized to 0 mV for 500 ms at time 0. Inset, somatic fluorescence was summed within the dotted line. (**b**) Basal $[Ca^{2+}]_{in}$ was averaged in the baseline period before depolarization. Average peak $[Ca^{2+}]_{in}$ was measured for 5 s starting from the peak. Neither parameter differed significantly between control and TTX-treated cells ($P > 0.2$). (**c**) Changes in eIPSC amplitudes after 500 ms depolarizations were recorded simultaneously with Ca^{2+} imaging. Black trace, average of eIPSCs before depolarization; gray trace, average of the second and third eIPSCs after depolarization. Bottom graph shows group data of DSI with 500 ms depolarization. The gray area represents integration of eIPSC suppression (the DSI integral) from 6 to 144 s. (**d**) DSI with 5 s depolarization to 0 mV. The DSI integral was obtained from the gray area in the range of 0–240 s. Gray trace, average of the first three eIPSCs after depolarization. (**e**) Group data of DSI integrals show no difference between control and TTX-treated groups with either 500 ms or 5 s depolarization ($P > 0.2$).

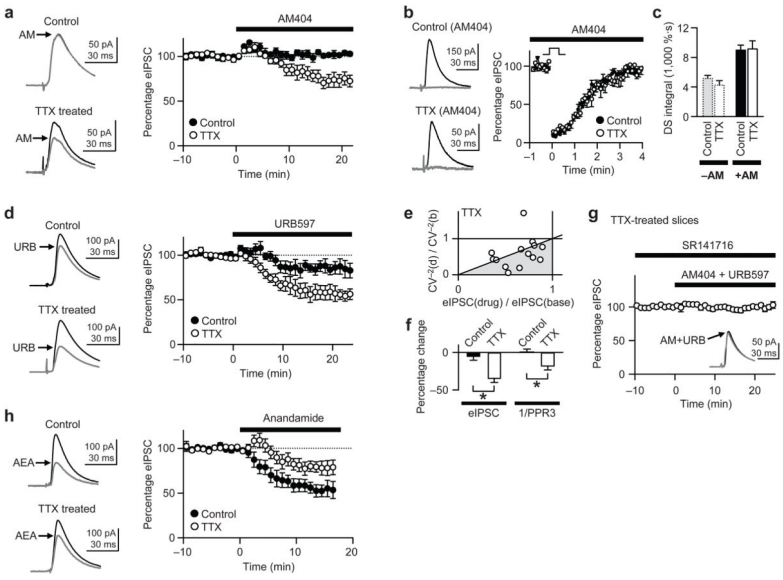

Figure 6.

Uptake and degradation of basal endocannabinoid are enhanced by activity deprivation. All slice cultures were preincubated with 300 nM ω-agatoxin IVA for 15–30 min. (**a**) AM404-mediated suppression of eIPSC is significantly larger in TTX-treated neurons than in control cells ($P < 0.005$). Right: representative traces of eIPSCs averaged before (black) and during (gray) application of 20 μM AM404, an endocannabinoid transporter inhibitor. (**b**) In the presence of AM404 (20 μM), the magnitudes of DSI (0 mV, 5 s) in control and TTX-treated cells were similar. Black traces, before depolarization; gray traces, average of the first three eIPSCs after depolarization. (**c**) DSI integral with 5 s depolarization did not differ between control and TTX-treated cells in the absence (−AM) or presence (+AM) of AM404, whereas AM404 increased DSI in each group. The dotted bars on the left were replotted from Figure 5e for comparison. (**d**) URB597-mediated suppression of eIPSC was significantly greater in TTX-treated cells than in control ($P < 0.02$). Right: representative traces of averaged eIPSCs showing the effect of 1 μM URB597 (gray traces). (**e**) From the data in **a** and **d**, the ratio of CV^{-2} in AM404 or URB597 to baseline CV^{-2} [CV^{-2}(drug)/CV^{-2}(base)] was plotted against the ratio of eIPSCs [eIPSC(drug)/eIPSC(base)]. Points in gray area and along the diagonal line imply presynaptic suppression of eIPSC by either AM404 or URB597. (**f**) The larger reduction in eIPSC amplitudes by AM404 or URB597 in TTX-treated cells is accompanied by a larger decrease in $PPR3^{-1}$, which is proportional to P_r. *, $P < 0.005$. (**g**) A cocktail of AM404 (20 μM) and URB597 (1 μM) did not suppress eIPSCs in the presence of 2 μM SR141716, indicating that AM404 and URB597 in **a** and **d** acted via CB1Rs. Inset: representative traces of averaged eIPSCs in the absence (black) or presence (gray) of the cocktail. (**h**) Bath-applied anandamide (720 nM) reduced eIPSCs to a lesser extent in TTX-treated cells than in control cells ($P < 0.05$). Right: averaged traces before and during (*AEA*) anandamide application. Ca^{2+} was excluded from the pipette solution to prevent FAAH from being occupied by endogenous anandamide.

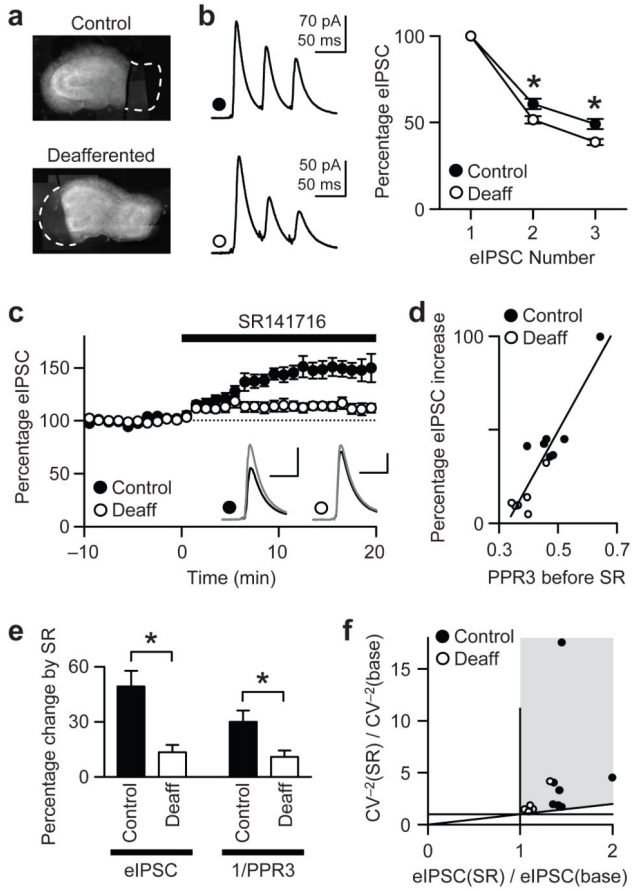

Figure 7.

Deafferentation of CA1 decreases tonic CB1R activity and increases basal GABAergic P_r, mimicking chronic TTX treatment. All slice cultures were incubated with ω-agatoxin IVA (300 nM) for 15–30 min prior to recording. (**a**) Micrographs of cultures from which CA3 or subiculum had been removed. CA3 removal eliminates afferent excitation of CA1 neurons, whereas subiculum removal serves as control. Dashed lines indicate the areas removed. (**b**) Short-term eIPSC depression (20 Hz) is more pronounced in deafferented slices than in control slices. Recordings were made 5–7 days after the cut. *, $P < 0.05$. (**c**) The increase in eIPSCs caused by SR141716 (2 μM) is larger in control cells than in deafferented cells ($P < 0.005$). Black trace, baseline; gray trace, SR141716. Amplitude scales, 50 pA for control and 100 pA for deafferented. Time scales, 30 ms. (**d**) When basal P_r is lower, as represented by higher PPR3 before SR141716, the SR141716-mediated increase in eIPSCs is larger. The line is a linear regression fit ($R^2 = 0.84$). (**e**) The larger enhancement in eIPSC amplitudes caused by SR141716 in control cells than in deafferented cells is accompanied by a larger increase in $PPR3^{-1}$. Data in **b** and **c** were analyzed. *, $P < 0.05$. (**f**) From the data in **c,** the ratio of CV^{-2} in SR141716 to baseline CV^{-2} [CV^{-2}(SR)/CV^{-2}(base)] is plotted against the ratio of eIPSCs. Points in gray area and along the diagonal line suggest presynaptic enhancement of transmission.

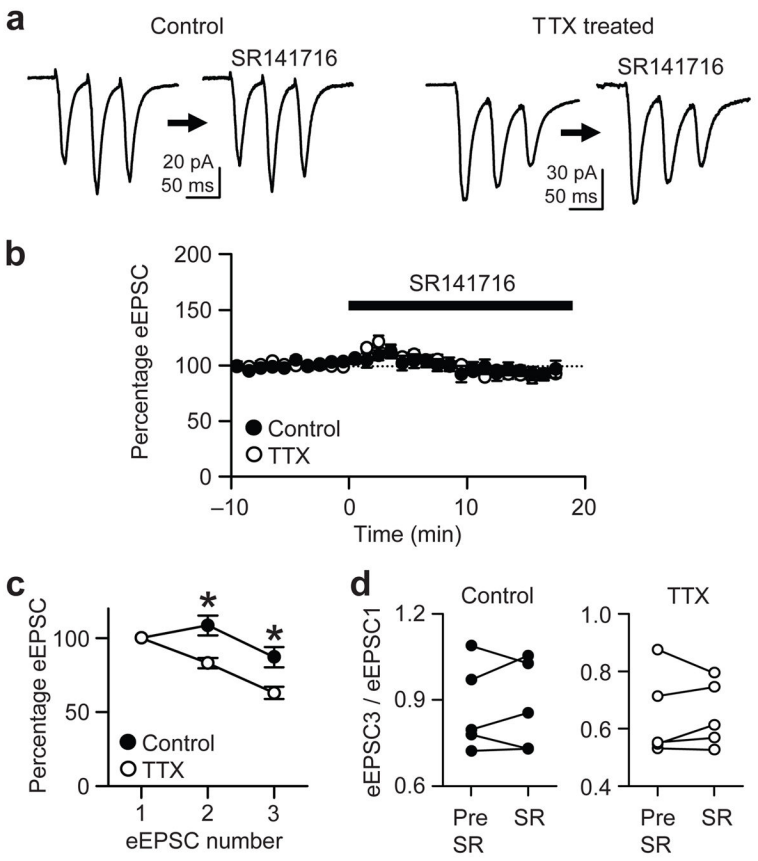

Figure 8.

Chronic TTX enhances P_r of excitatory synapses independently of tonic endocannabinoid action. (**a**) Averaged traces of eEPSCs before and during SR141716 (2 μM) application. SR141716 had no effect on the amplitude of eEPSCs recorded from CA1 pyramidal neurons. (**b**) Group data, normalized to pre-SR141716 baseline, show that SR141716 caused no significant changes in eEPSCs in either treatment group. (**c**) Short-term plasticity of eEPSC was assessed with 20 Hz stimulation. TTX-treated cells displayed more rapid depression. The second and the third eEPSCs were normalized to the first eEPSC amplitude. *, $P < 0.005$. (**d**) The ratios of eEPSC3/eEPSC1 were not significantly different before (*Pre-SR*) or in the presence of (*SR*) 2 μM SR141716 in either treatment group, implying the increased glutamatergic P_r (represented by eEPSC3/eEPSC1) was independent of CB1Rs. Each dot indicates individual cell.